EFFECT OF STRUCTURAL VARIATIONS ON THERMAL DEFORMATION OF SINGLE CURVATURE COMPOSITE SANDWICH PANELS

by

BRADY C. LOTZ

Presented to the Faculty of the Graduate School of

The University of Texas at Arlington in Partial Fulfillment

of the Requirements

for the Degree of

MASTER OF SCIENCE IN MECHANICAL ENGINEERING

THE UNIVERSITY OF TEXAS AT ARLINGTON

May 2016

Supervising Committee:

Dr. Wen S. Chan
Dr. Kent L. Lawrence
Dr. Ashfaq Adnan

Acknowledgements

I would like to thank Dr. Chan for his help and encouragement while completing this thesis. His knowledge of composite structures was a much needed and appreciated resource.

I would also like to thank my soon-to-be wife, Charlene, for believing in me and pushing me to finish this thesis and degree in a timely manner.

April 20, 2016

Abstract

EFFECT OF STRUCTURAL VARIATIONS ON THERMAL DEFORMATION
OF SINGLE CURVATURE COMPOSITE
SANDWICH PANELS

Brady C. Lotz, M.S.

The University of Texas at Arlington, 2016

Supervising Professor: Wen S. Chan

Composite structures cured at a high temperature in a contoured female mold have a tendency to deform or spring-in when brought down to room temperature from cure temperature. This thesis investigates the effects of various structural parameters on the spring-in of the curved shape of a composite sandwich panel due to thermal deformation. A finite element model of a single curved composite sandwich panel is developed using 3D shell elements and validated against other published articles and classical lamination theory. Using a control structure of AS4/3501-6 carbon/epoxy with half inch Nomex honeycomb core with a layup of $[0°/90°/0°/90°/Core/90°/0°/90°/0°]_T$, structural parameters are varied including core thickness, face sheet thickness, face sheet ply orientation, asymmetric face sheets, temperature delta, and structure radius. Core thickness variations using the control layup were found to decrease the total spring-in as core thickness (as well as bending stiffness) increased; however, as face sheet thickness increases for a constant core thickness, total spring-in increases. Cases using other quasi-isotropic face sheets other than 0°/90° layups were analyzed and found to correspond to the results from the face sheet thickness study.

Table of Contents

List of Figures

List of Tables

Chapter 1

Introduction

1.1 Composite Sandwich Panel Background

Simply stated, a composite is a material composed of more than one distinct constituent material. Fiber reinforced polymer composites are used to take the high stiffness and strength properties of a fiber material such as graphite, glass, or aramid and bind the fibers in specific orientations with the polymer matrix in order to more efficiently resist loads acted upon the structure. Sandwich panels consist of two thin outside layers, or face sheets, separated by and bonded to a thicker, lighter-weight core material. This creates a structure similar to an I-beam, with the face sheets analogous to the stiff top and bottom I-beam flanges and the core material analogous to the I-beam's shear web. Sandwich panels are used where high bending stiffness is required with minimum weight. Low weight for a given stiffness is achieved by increasing the thickness of the core material which is often lighter and lower cost than the face sheet material. Core materials are commonly a lightweight honeycomb structure with hexagonal, thin-walled cells made of materials such as aluminum, fiberglass, or the aramid polymer Nomex. Honeycomb cores may come in various configurations that make the material easier to flex in certain directions. Closed-cell foam is also commonly used as a core material in composite sandwich panels. Face sheets are made of materials with high strength such as a metal plate or fiber reinforced polymer composite. A sandwich panel with composite face sheets takes advantage of the high specific bending stiffness of a sandwich panel and combines it with the high specific strength of the composite material to create a very weight efficient structure.

The manufacturing of composite sandwich panels is similar to that of other laminated composites. A mold is created in the form of the final part shape (or a modified

shape taking into account the deformations caused by thermal effects during the curing process), usually in a female configuration with the tool surface representing the outer surface of the final structure. All constituent parts of the sandwich panel can be co-cured in one cure cycle using prepreg fiber/epoxy plies. When curing everything at once, adhesive is not needed to bond the core to the face sheets because the resin in the prepreg acts as the bonding agent. The entire assembly can then be cured using a vacuum bag and autoclave similar to other laminated composite parts, but at a lower pressure depending on the core material. High pressures from an autoclave may crush certain core materials or draw the inner face sheet laminate into the cells of a honeycomb core creating a wrinkle in the face sheet therefore reducing the stiffness, strength, and life of the structure. Co-curing the sandwich panel assembly will increase the void content of the face sheets because proper consolidation cannot occur due to the reduced cure pressure. Another option for manufacturing composite sandwich panels is to cure the face sheets separately at the proper pressure for complete consolidation. The core material can then be bonded to each pre-cured face sheet with adhesive layers. Independent curing of the face sheets is ideal for flat sandwich panels, but is very difficult to achieve for panels with any type of contour since the inner face sheet shape is difficult to determine. This leads to one more manufacturing option for contoured sandwich panels. The outer face sheet can be cured and consolidated on the mold by itself to achieve minimum void content. The core can then be bonded to the outer face sheet using an adhesive layer in a separate cure cycle with the inner face sheet. This modified process will ensure that void content is reduced where possible.

The manufacturing process of composite materials has many opportunities to introduce deformation into the final part shape. This deformation is a problem because the effects are difficult to compensate for prior to manufacturing the part. The final

deformation is difficult to predict and is a factor of many different variables including constituent materials and their orientation, cure cycles and temperatures, and tool shape and material. This paper focuses on only one cause of deformation: spring-in. The tendency for a curved composite structure to pull away from a female mold as the structure cools to room temperature from its cure temperature is commonly referred to as spring-in. Spring-in is primarily the result of thermal deformation due to this change in temperature. An angled or curved composite structure cured on a tool with a given angle or radius will result in a final part shape with a smaller angle or smaller radius than the tool shape. The decrease of this angle or radius corresponds to an increase in spring-in.

1.2 Literature Survey

Many research papers investigate the deformation of laminated composites to try to better understand this issue, but few papers are available that look into the thermal deformation of composite sandwich panels.

Albert and Fernlund [1] experimentally tested L- and C-shaped laminated composite structures for spring-in and warpage due to process-induced effects and structural effects, which the paper refers to as extrinsic and intrinsic parameters. The authors use a fractional factorial experiment design approach which allows them to test eight different factors while minimizing the number of test cases. In the conclusion of the paper, the authors give a rating of the importance of each tested parameter on spring-in and found that part thickness and part length are of great importance, and part layup and angle were of medium importance for the tested shapes.

Later, Fernlund [2] focused on the spring-in of 90° composite sandwich panels consisting of two planar flange sections oriented 90° to one another and joined by a constant radius section. An analytical model for predicting the spring-in of 90° angled sandwich panels was developed, and the model was validated by finite element analysis

for the sandwich structure with different core materials. The main idea of Ferlund's investigation is that the resulting thermally deformed angle is primarily the result of the difference in the thermal expansion in the in-plane and thickness directions.

Recently, Mahadik and Potter [3] experimentally determined the spring-in of one layup of a curved composite sandwich panel with foam core. Spring-in was measured as the distance between each tip point at room temperature and an elevated 100° C to simulate the structure before cure cooldown. Mahadik and Potter found that 95%-98% of the spring-in was recovered by reheating when compared to the tool shape. This demonstrates that only a small amount of distortion is caused by non-thermoelastic effects including cure shrinkage and tool-part friction. A finite element model was then developed in ANSYS which was found to agree closely with the experimental results. Mahadik and Potter also concluded that the spring-in from thermal deformation is primarily the result of the difference in thermal expansion in the in-plane and thickness directions similar to Fernlund's [2] findings.

Black et al. [4] experimentally investigated the spring-in behavior of different thick L-shaped graphite/epoxy angle laminates. They first tested varying thicknesses of $[0°/90°]_{xs}$ and $[45°/-45°]_{xs}$ layups and found that spring-in decreases as laminate thickness increases. They then looked at angle ply layups of the form $[\theta_4°/-\theta_4°]_s$, and found the most spring-in for the $[\theta_4°/-\theta_4°]_s$ specimen, the least spring-in at $[0°]_{16T}$, and also a low spring-in value for $[90°]_{16T}$. Ply packs of $[0°/90°]_{4s}$ and $[45°/-45°]_{4s}$ were compared to interspersed plies of $[(0°)_4/(90°)_4]_s$ and $[(45°)_4/(-45°)_4]_s$. It was found that spring-in was not affected by using ply packs versus interspersed plies unless there is a significant different in bending stiffness between the two compared layups.

Kappel [5] validates two analytical models that predict composite structure spring-in, including Ferlund's model [2], for curved composite sandwich panels with

Rohacell foam core using experimental tests. He also created a novel simulation technique using his experimental results as input. Kappel also demonstrates with experimental tests that spring-in decreases as core thickness increases for his specific structure with $[0°/90°]_4$ face sheets. Chamfered and open core runout designs were also tested to determine if spring-in was affected, but no significant differences in spring-in were observed with the laminates used in this study.

1.3 Thesis Objective

The objective of this thesis is to investigate the effects of various structural parameters on the spring-in of the curved shape of a composite sandwich panel due to thermal deformation. In order to investigate the effects, a finite element model of a single curved composite sandwich panel will be developed and validated against other published articles.

Specific tested structural parameters include core thickness, face sheet thickness, face sheet ply orientation, asymmetric face sheet thickness, and structure radius. This study hopes to draw general conclusions on the effects of these parameters on the spring-in of the composite sandwich panel.

1.4 Thesis Outline

Chapter 2 details the development of the finite element model used in this thesis. This includes the element type selection, mesh creation, boundary conditions, and application of loads. The model is then validated with a comparison to results in a published paper.

Chapter 3 discusses classical lamination theory, thermal induced forces and moments, and how laminate bending stiffness can be calculated analytically.

Chapter 4 discusses the results of each investigated parameter in this study. Data is tabulated and graphed to display general trends that are used to draw general conclusions.

Chapter 5 summarizes the general conclusions that can be made from the cases investigated in this study.

Chapter 2

Finite Element Analysis

A finite element model will be used to investigate the effect of varying material parameters on the thermal deformation of a curved composite sandwich panel. ANSYS Mechanical ADPL 16.2 is used to construct this model.

2.1 Problem Definition

The geometry of the composite sandwich panel used in this thesis was chosen for its similarity to structures used for external fairings and radomes in the aerospace industry. The finite element model thickness will be on the order of 0.5 inches thick and 50 inches long around a 16-inch radius by 24 inches wide. The objective is to create a finite element model that can be used to accurately model spring-in of the curved sandwich panel structure due to thermoelastic effects.

2.2 Element Type Selection

Element types must be considered before constructing the model. Shell elements and 3D elements require different meshes: a 3D surface and a 3D volume, respectively. Shell elements were chosen because they can be used to efficiently model thin structures that have one dimension (thickness for example) which is significantly smaller than the other two dimensions (length and width) [6]. The small thickness dimension of the geometry used here relative to the length and width of the structure is ideal for using shell elements, but care must be taken not to decrease the size of the elements smaller than the thickness of the structure because unrealistic deflections will result. The ANSYS Mechanical APDL Element Reference Guide [6] states that “shell elements decouple the deformation on the surface and the deformation in the normal direction, allowing for a simple and efficient simulation of a thin structure.” The unrealistic behavior that occurs when the element aspect ratio is small is the result of this decoupling.

Two shell elements were considered for the sandwich panel finite element model: SHELL181 and SHELL281. The SHELL181 element is a 4-node shell element with one node at the mid-thickness of each of the four corners of the element. This element has six degrees-of-freedom at each node: three translational degrees-of-freedom along the x, y, z axes and three rotational degrees-of-freedom about the x, y, z axes. The SHELL281 element is an 8-node shell element with four nodes (I,J,K,L in Figure 2-1) at the mid-thickness of each of the four corners of the element and four nodes (M,N,O,P in Figure 2-1) at the midpoints between the four corner nodes. These midpoint nodes allow for greater edge warping for more realistic results. The SHELL281 element has six degrees-of-freedom at each node just like the SHELL181 element. Both element types can have an initial temperature property applied, which will be affected by a thermal load. Figure 2-1 below shows a typical SHELL281 element, its node locations, and coordinate system.

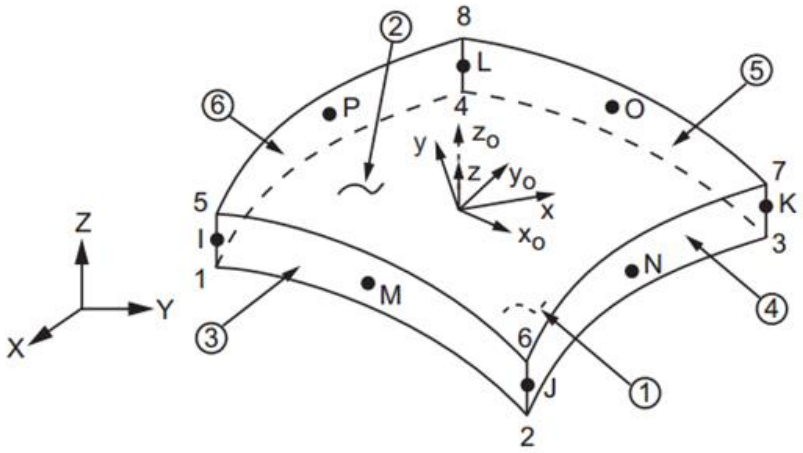

Figure 2-1 ANSYS SHELL281 Element [6]

Using the SHELL181 element, the spring-in effect was not noticeable when the model was subjected to a thermal load. Table 2-1 shows a comparison between the measured spring-in gap (larger numbers equate to more spring-in) of SHELL181 elements versus SHELL281 elements with three different core thicknesses. It can be

seen that no difference in spring-in gap is found for any of the three test cases using the SHELL181 element. No change in deformation under thermal load with varying structure is not an acceptable result and therefore another element must be used.

Table 2-1 Comparison between SHELL181 and SHELL281 spring-in gap results for varying core thickness

Layup	SHELL181 Gap	SHELL281 Gap
$[0°/90°/0°/90°/0.5Core/90°/0°/90°/0°]_T$	1.201E-03	3.121E-02
$[0°/90°/0°/90°/0.25Core/90°/0°/90°/0°]_T$	1.201E-03	3.143E-02
$[0°/90°/0°/90°/0.1Core/90°/0°/90°/0°]_T$	1.201E-03	3.188E-02

As shown in Table 2-1, it is apparent that the SHELL281 element yields a trend in measured spring-in gap as core thickness is varied, unlike the SHELL181 element which shows no variation. Therefore, the SHELL281 element will be used in all finite element model cases investigated in this paper hereinafter.

Shell elements, including SHELL281, can be defined with multiple sections or layers. This allows for a 2D surface to have meshed shell elements with individual layers, each having different properties, thicknesses, and orientations. For the composite sandwich panel model, there will be one layer for each fiber/matrix lamina and one layer for the core material. An example section property definition for a $[0°/90°/0°/90°/Core/90°/0°/90°/0°]_T$ layup is pictured in Figure 2-2. Material 1 represents a single face sheet ply and Material 2 represents the core material.

	Thickness	Material ID	Orientation	Integration Pts	Pictorial View
9	0.005	1	0	3	
8	0.005	1	90	3	
7	0.005	1	0	3	
6	0.005	1	90	3	
5	0.5	2	0	3	
4	0.005	1	90	3	
3	0.005	1	0	3	
2	0.005	1	90	3	
1	0.005	1	0	3	

Figure 2-2 ANSYS 16.2 Sample section definition

2.3 Mesh Construction

To construct the mesh, a 3D surface in the shape to be studied must first be created. A 180° constant 16-inch radius arc was drawn and extruded 24 inches to create the basic 3D surface. This surface was then meshed using the default MeshTool settings in ANSYS. The Mesh was further refined to a 24x48 element mesh with the MeshTool resulting in the progression show in Figure 2-3. The SHELL281 element type with the section properties discussed previously are applied to the entire mesh.

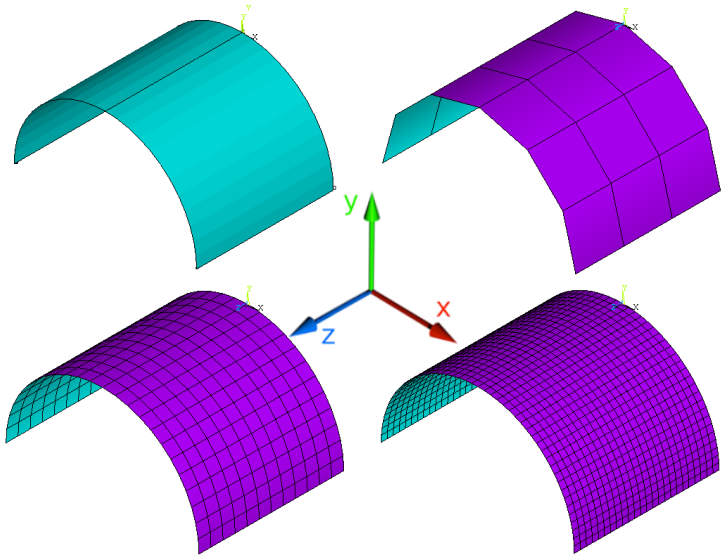

Figure 2-3 Progression of the mesh using MeshTool in ANSYS Preprocessing

The element section orientations (listed in Figure 2-2) that represent individual lamina are relative to the global laminate coordinate system as defined in Section 3.1,

which is different from the model coordinate system shown in Figure 2-3. This difference in coordinate systems is shown in Figure 2-4. Also, since this structure is curved in one direction, the laminate coordinate system rotates about the x-axis such that the z-direction remains normal to the shell surface.

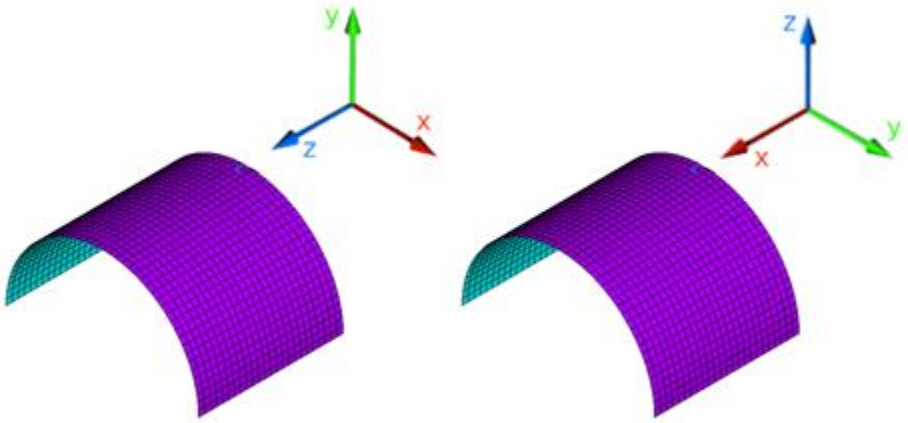

FE Model Laminate

Figure 2-4 Model coordinate system compared to laminate coordinate system

For shell elements, the aspect ratio (length/thickness) must be considered when selecting a mesh size. The length of the element must be larger than the thickness of the material defined by the shell element for the model to produce realistic results. Table 2-2 lists the aspect ratio of the elements shown in the mesh progression in Figure 2-3 using the lengths in both the x and y laminate directions and a 0.54-inch thickness. The 24x48 element mesh approaches a 1:1 ratio of length (L) to thickness (t). Another doubling of elements would surpass this limit and begin to negatively affect the model accuracy.

Table 2-2 Aspect ratio of element length vs. thickness

Elements	L_x/t	L_y/t
3x6	14.81	15.51
12x24	3.70	3.88
24x48	1.85	1.94

A 24x48 element mesh was selected based on a mesh size study (shown in Figure 2-5) that resulted in choosing the smallest mesh that does not sacrifice model accuracy and does not have an aspect ratio less than one. In the study, the mesh size was increased until the results approximately plateaued to some value and more elements no longer resulted in a more accurate value. Using more elements than 24x48 takes more processing time and does not change the result significantly.

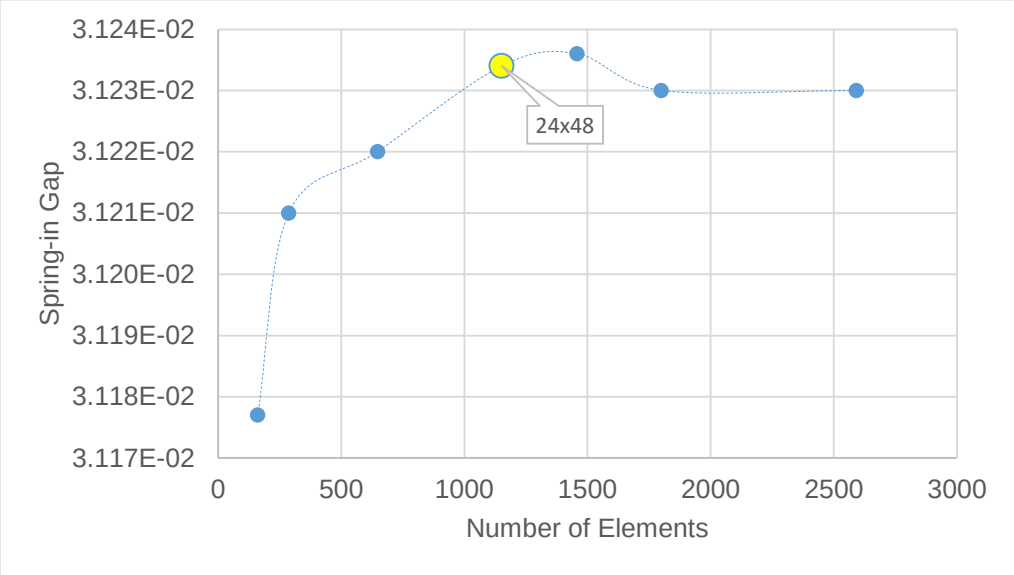

Figure 2-5 Mesh size study showing resulting spring-in gap of one case plateauing around the 24x48 mesh size

2.4 Material Properties

The materials used in this study are AS4/3501-6 carbon/epoxy lamina and HRH-10-3/8-3.0 Nomex honeycomb core unless otherwise noted. The 3D material properties for the carbon/epoxy lamina are taken from Ref. [7]. The Nomex honeycomb core material data was found in Refs. [8] and [9]. Not all 3D properties for the core material is available within these two documents, and therefore some properties were given arbitrarily low values per Hexcel's *Honeycomb Sandwich Design Technology* document

[10] that discusses computer modeling of honeycomb sandwich panels. The properties used for both materials are listed below in Table 2-3.

Table 2-3 Material properties used throughout this study [7],[8],[9],[10]

Property	**AS4/3501-6 Carbon/Epoxy Lamina**	**HRH-10-3/8-3.0 Nomex Core**
Longitudinal modulus, E_1, Msi	21.3	0.00001*
Transverse in-plane modulus, E_2, Msi	1.50	0.00001*
Transverse out-of-plane modulus, E_3, Msi	1.50	0.017
In-plane Poisson's ratio, v_{12}	0.27	0.1
Out-of-plane Poisson's ratio, v_{23}	0.54	0.01*
Out-of-plane Poisson's ratio, v_{13}	0.27	0.01*
In-plane shear modulus, G_{12}, Msi	1.00	0.00001*
Out-of-plane shear modulus, G_{23}, Msi	0.54	0.0035
Out-of-plane shear modulus, G_{13}, Msi	1.00	0.0056
Longitudinal CTE, α_1, 10^{-6}/°F	-0.5	0.01*
Transverse CTE, α_2, 10^{-6}/°F	15	0.01*
Out-of-plane CTE, α_3, 10^{-6}/°F	15	19.4
Thickness, *t*, in.	0.005	-

*Values set arbitrarily low per [10]

2.5 Boundary Conditions

A single all-degree-of-freedom (translation and rotation) constraint was placed at the center node at the top of the arc on one side of the cross-section to allow free deformation about that point as shown in Figure 2-6. This constraint node is also set as the origin of the system so that all measured deflections will be relative to this constrained point. This will allow deflections at the corner nodes to be easily compared. No additional constraints are required. If additional constraints were added, they would constrain the geometry and cause non-uniform stress.

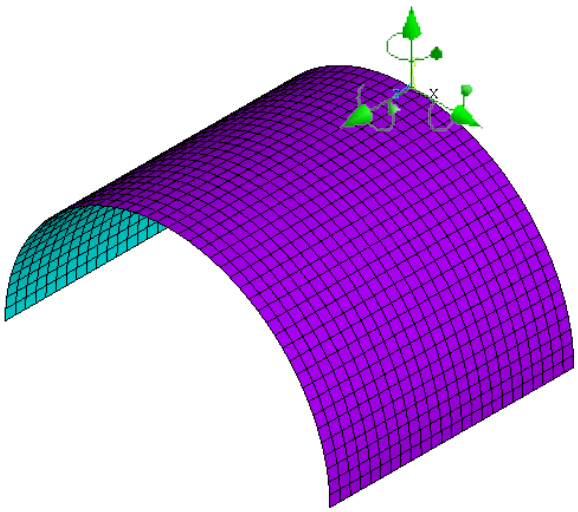

Figure 2-6 One all-degree-of-freedom constraint applied at the origin

2.6 Thermal Loading

A -50° Fahrenheit change in temperature was then applied to the entire model surface to simulate the temperature change and resulting deformation that a composite material would undergo when the matrix has reached its cure temperature and is then brought down to room temperature. This -50°F is used for all cases in this paper unless stated otherwise.

2.7 Spring-in Measurement

Spring-in will be measured by adding together the nodal deflections in the x-direction of each tip away from the origin to give the total spring-in. This measurement is equivalent to measuring the nominal tip-to-tip distance and subtracting the deformed tip-to-tip distance to arrive at the total spring-in as depicted in Figure 2-7. The nodal deflections are obtained from ANSYS General Postproc > List Results > Nodal Solution at the nodes located at the tip corners.

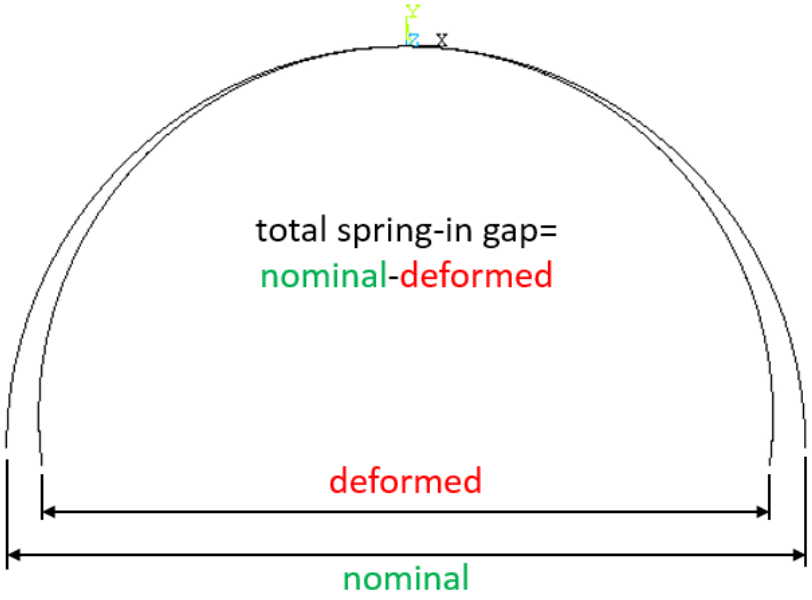

Figure 2-7 Nominal and deformed tip-to-tip measurements subtracted to arrive at the total spring-in gap measurement for $\Delta T < 0$

2.8 FEM Validation

The previously described finite element model was validated against Mahadik and Potter's [3] curved composite sandwich panel experimental results. All of Mahadik and Potter's test specimens were constructed using the same dimensions and ply stack up. The specimens all measured a 400mm radius and 200mm in length with a layup of $[0°/90°/Core/90°/0°/Resin]_T$ with a resin rich layer on the tool-side of the laminate and were subjected to a -100°C change in temperature. The core thickness used was 10mm and the ply thickness measured 0.25mm. The finite element model previously described in Sections 2.2 through 2.6 was modified to use the same dimensions and material properties as Mahadik and Potter's experiment (Table 2-4). It should be noted that Mahadik and Potter's material properties appear to have incorrect values for Poisson's ratios and shear moduli. For a fiber/epoxy composite material, ν_{12} should equal ν_{13} and

G_{12} should equal G_{13}. The results were calculated with both the displayed material properties and the corrected values and the difference was found to be negligible.

Table 2-4 Verification Material Properties [3]

Property	**Glass Lamina**	**Foam Core**	**Resin**
Longitudinal modulus, *E₁*, Msi (GPa)	5.22 (36)	0.0087 (0.060)	1.31 (9.0)
Transverse in-plane modulus, *E₂*, Msi (GPa)	1.43 (9.862)	0.0087 (0.060)	1.31 (9.0)
Transverse out-of-plane modulus, *E₃*, Msi (GPa)	1.43 (9.862)	0.0087 (0.060)	1.31 (9.0)
In-plane Poisson's ratio, *ν₁₂*	0.303	0.21	0.3
Out-of-plane Poisson's ratio, *ν₂₃*	0.303	0.21	0.3
Out-of-plane Poisson's ratio, *ν₁₃*	0.259	0.21	0.3
In-plane shear modulus, *G₁₂*, Msi (GPa)	0.431 (2.971)	0.00319 (0.022)	0.305 (2.10)
Out-of-plane shear modulus, *G₂₃*, Msi (GPa)	0.311 (2.144)	0.00319 (0.022)	0.305 (2.10)
Out-of-plane shear modulus, *G₁₃*, Msi (GPa)	0.311 (2.144)	0.00319 (0.022)	0.305 (2.10)
Longitudinal CTE, *α₁*, 10^{-6}/°F (10^{-6}/°C)	4.24 (7.63)	55.6 (100)	27.8 (50)
Transverse CTE, *α₂*, 10^{-6}/°F (10^{-6}/°C)	24.4 (43.9)	55.6 (100)	27.8 (50)
Out-of-plane CTE, *α₃*, 10^{-6}/°F (10^{-6}/°C)	27.8 (50.0)	55.6 (100)	27.8 (50)
Thickness, *t*, in. (mm)	0.00984 (0.25)	0.394 (10)	0.000787 (0.020)

The results of the 3D finite element shell model defined in this paper using Mahadik and Potter's dimensions and properties are shown in Figure 2-8 alongside Mahadik and Potter's experimental results and finite element model results. The effect of adding the resin rich layer to the model is depicted as a reduction in the overall spring-in of the structure (shown in orange). The results of this finite element model for this specific structure is shown to be within 5.9% of Mahadik and Potter's experimental result average and within 4.6% of Mahadik and Potter's finite element model result.

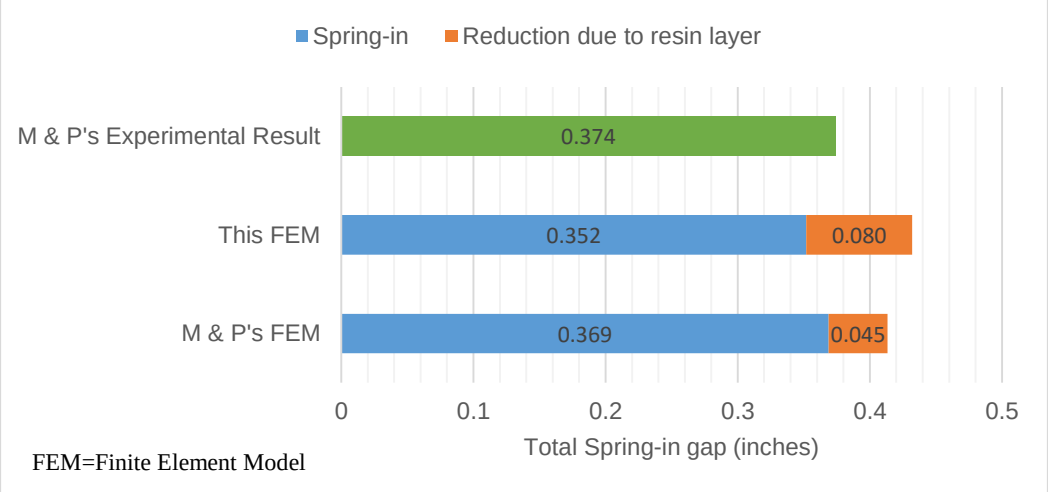

Figure 2-8 Bar graph summarizing the comparison of this paper's FEM results to experimental and FEM results from Mahadik and Potter [3]

Chapter 3

Lamination Theory

Lamination theory can be used to calculate stresses and strains on individual lamina from applied forces and moments or strains using a multi-layered laminated composite structure's material properties and constituent lamina orientations. This chapter will give a brief summary of lamination theory.

3.1 Lamina and Laminate Coordinate Systems

There are two different coordinate systems used in classical lamination theory. First, there is the individual lamina with axis directions labeled 1, 2, and 3. The 1- and 2-directions represent the plane of the lamina with the 1-direction representing the primary fiber direction and the 2-direction representing the transverse in-plane direction. The 3-direction then represents the transverse out-of-plane direction. Each lamina in a laminate has its own lamina coordinate system.

Second, there is the laminate coordinate system that is a shared global coordinate system which uses x, y, and z axes. All the individual lamina coordinate systems must be transformed into this global laminate coordinate system. For a flat plate laminate, x- and y-directions are commonly in the plane of the plate with the x-direction corresponding to the 0° fiber direction. The z-direction represents the normal vector of the flat plate. An angle ply rotated θ° about the plane of the plate will be rotated θ° about the z-axis toward the y-axis. This rotation is counter-clockwise when looking at the top of the plate with the z-direction representing the up direction. The two coordinate systems can be seen in Figure 3-1 for a single lamina rotated θ° about the z-axis. The origin of the global laminate coordinate system is commonly placed at the mid-plane of the laminate located at the middle of its thickness.

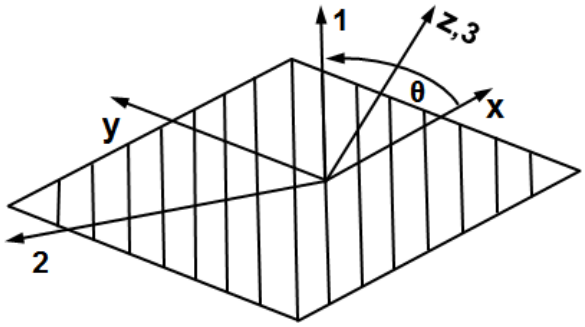

Figure 3-1 Lamina and laminate coordinate systems for one angled ply [11]

3.2 Stress/Strain Relationship of Elastic Solids

Using Hooke's law of relating stress to strain ($\sigma = c\varepsilon$), an equation can be written that relates stress to strain in all three spatial directions using a stiffness matrix [*c*]. This stiffness matrix for a general anisotropic material has 21 independent constants.

$$\begin{Bmatrix} \sigma_1 \\ \sigma_2 \\ \sigma_3 \\ \tau_{23} \\ \tau_{13} \\ \tau_{12} \end{Bmatrix} = \begin{bmatrix} c_{11} & c_{12} & c_{13} & c_{14} & c_{15} & c_{16} \\ & c_{22} & c_{23} & c_{24} & c_{25} & c_{26} \\ & & c_{33} & c_{34} & c_{35} & c_{36} \\ & & & c_{44} & c_{45} & c_{46} \\ & sym & & & c_{55} & c_{56} \\ & & & & & c_{66} \end{bmatrix} \cdot \begin{Bmatrix} \varepsilon_1 \\ \varepsilon_2 \\ \varepsilon_3 \\ \gamma_{23} \\ \gamma_{13} \\ \gamma_{12} \end{Bmatrix} \tag{3-1}$$

This relationship can also be written using a compliance matrix [*s*] where [*s*]=[*c*]$^{-1}$.

$$\begin{Bmatrix} \varepsilon_1 \\ \varepsilon_2 \\ \varepsilon_3 \\ \gamma_{23} \\ \gamma_{13} \\ \gamma_{12} \end{Bmatrix} = \begin{bmatrix} s_{11} & s_{12} & s_{13} & s_{14} & s_{15} & s_{16} \\ & s_{22} & s_{23} & s_{24} & s_{25} & s_{26} \\ & & s_{33} & s_{34} & s_{35} & s_{36} \\ & & & s_{44} & s_{45} & s_{46} \\ & sym & & & s_{55} & s_{56} \\ & & & & & s_{66} \end{bmatrix} \cdot \begin{Bmatrix} \sigma_1 \\ \sigma_2 \\ \sigma_3 \\ \tau_{23} \\ \tau_{13} \\ \tau_{12} \end{Bmatrix} \tag{3-2}$$

This anisotropic equation can be simplified if a structure has planes of symmetry. A unidirectional lamina can be considered orthotropic if it has three perpendicular planes of symmetry relative to its material properties. A unidirectional lamina can be further

simplified into a transversely isotropic material in which two of the three planes of symmetry share the same material properties. A transversely isotropic material has five independent material constants (s_{44} is not an independent constant).

$$\begin{Bmatrix} \varepsilon_1 \\ \varepsilon_2 \\ \varepsilon_3 \\ \gamma_{23} \\ \gamma_{13} \\ \gamma_{12} \end{Bmatrix} = \begin{bmatrix} s_{11} & s_{12} & s_{12} & 0 & 0 & 0 \\ & s_{22} & s_{23} & 0 & 0 & 0 \\ & & s_{22} & 0 & 0 & 0 \\ & & & s_{44} & 0 & 0 \\ & sym & & & s_{55} & 0 \\ & & & & & s_{55} \end{bmatrix} \cdot \begin{Bmatrix} \sigma_1 \\ \sigma_2 \\ \sigma_3 \\ \tau_{23} \\ \tau_{13} \\ \tau_{12} \end{Bmatrix} \tag{3-3}$$

For a thin lamina, the plane stress condition can be used to further simplify this equation. The plane stress condition is the state where stress and shear stress in the out-of-plane direction are assumed zero ($\sigma_3 = \tau_{13} = \tau_{23} = 0$). This simplified compliance matrix [*s*] is called the reduced compliance matrix, which only has four independent material properties S_{11}, S_{12}, S_{22}, and S_{66} that are related to E_1, E_2, G_{12}, and v_{12}.

$$\begin{Bmatrix} \varepsilon_1 \\ \varepsilon_2 \\ \gamma_{12} \end{Bmatrix} = \begin{bmatrix} s_{11} & s_{12} & 0 \\ & s_{22} & 0 \\ sym & & s_{66} \end{bmatrix} \cdot \begin{Bmatrix} \sigma_1 \\ \sigma_2 \\ \tau_{12} \end{Bmatrix} \text{ or } \{\varepsilon\}_{1-2} = [s]_{1-2} \cdot \{\sigma\}_{1-2} \tag{3-4}$$

This equation can also be written with a reduced stiffness matrix [*Q*] where $[Q]=[s]^{-1}$.

$$\begin{Bmatrix} \sigma_1 \\ \sigma_2 \\ \tau_{12} \end{Bmatrix} = \begin{bmatrix} Q_{11} & Q_{12} & 0 \\ & Q_{22} & 0 \\ sym & & Q_{66} \end{bmatrix} \begin{Bmatrix} \varepsilon_1 \\ \varepsilon_2 \\ \gamma_{12} \end{Bmatrix} \tag{3-5}$$

The values of the constituent terms in matrices [*s*] and [*Q*] are shown in Equation (3-6).

$$
\begin{aligned}
s_{11} &= \frac{1}{E_1} \\
s_{22} &= \frac{1}{E_2} \\
s_{12} &= -\frac{\nu_{12}}{E_1} \\
s_{66} &= \frac{1}{G_{12}} \\
Q_{11} &= \frac{E_1}{1-\nu_{12}\nu_{21}} \\
Q_{22} &= \frac{E_2}{1-\nu_{12}\nu_{21}} \\
Q_{12} &= \frac{E_1\nu_{21}}{1-\nu_{12}\nu_{21}} \\
Q_{66} &= G_{12}
\end{aligned}
\tag{3-6}
$$

3.3 Transformation Between Coordinate Systems

As mentioned previously, it is necessary to transform every lamina into the global laminate coordinate system. Once the reduced stiffness matrix $[Q]_{1-2}$ for an individual lamina is calculated, this matrix can be transformed into the global laminate coordinate system as $[\bar{Q}]_{x-y}$.

$$[\bar{Q}]_{x-y} = [T_\sigma(-\theta)] \cdot [Q]_{1-2} \cdot [T_\varepsilon(\theta)] \tag{3-7}$$

The two matrices mentioned in Equation (3-7) are transformation matrices used to transform stresses and strains in the x-y coordinate system to the 1-2 coordinate system. These transformation matrices can be used at the end of the calculations to transform laminate stresses and strains back into local lamina stresses and strains for failure analysis.

$$[\sigma]_{1-2} = [T_\sigma(\theta)] \cdot [\sigma]_{x-y} \tag{3-8}$$

$$[\varepsilon]_{1-2} = [T_\varepsilon(\theta)] \cdot [\varepsilon]_{x-y} \tag{3-9}$$

$$[T_\sigma(\theta)] = \begin{bmatrix} m^2 & n^2 & 2mn \\ n^2 & m^2 & -2mn \\ -mn & mn & m^2 - n^2 \end{bmatrix} \tag{3-10}$$

$$[T_\varepsilon(\theta)] = \begin{bmatrix} m^2 & n^2 & mn \\ n^2 & m^2 & -mn \\ -2mn & 2mn & m^2 - n^2 \end{bmatrix} \tag{3-11}$$

Where $m = \cos\theta$ and $n = \sin\theta$.

3.4 Hygrothermal Strain

Hygrothermal strain is strain caused by temperature and moisture content changes. Both of these effects are treated the same mathematically. A change in temperature (ΔT) along with the coefficient of thermal expansion (CTE) of a particular material can be used to determine the induced normal strain in the lamina coordinate system. No shear strains are induced by hygrothermal effects for a 0° lamina. These induced strains can be added to other strains caused by external forces.

$$\begin{Bmatrix} \varepsilon_1^T \\ \varepsilon_2^T \\ 0 \end{Bmatrix} = \begin{Bmatrix} \alpha_1 \\ \alpha_2 \\ 0 \end{Bmatrix} \cdot \Delta T \tag{3-12}$$

Where $\alpha = CTE$.

Since the hygrothermal strains are initially in the lamina coordinate system, they must be converted to the laminate coordinate system to be used for laminate calculations using the same strain transformation matrix $[T_\varepsilon(\theta)]$ given in Section 3.3. However, when converting from the lamina coordinate system to the laminate coordinate system, the inverse of the transformation matrix must be used as shown in Equation (3-13). Conveniently the inverse of $[T_\varepsilon(\theta)]$ is simply $[T_\varepsilon(-\theta)]$.

$$[\varepsilon^T]_{x-y} = [T_\varepsilon(-\theta)] \cdot [\varepsilon^T]_{1-2} \tag{3-13}$$

3.5 Classical Lamination Theory

Once all constituent lamina of a composite laminate are converted to the global laminate coordinate system, the mechanical stress/strain relationship in a temperature environment can be written for each layer *k* relative to the mid-plane strain $[\varepsilon^0]$, distance from the mid-plane *z*, and the mid-plane curvature $[K]$ as shown in Equation (3-14).

$$\left[\sigma_{x-y}\right]_k = \left[\bar{Q}_{x-y}\right]_k \cdot \left(\left[\varepsilon^0_{x-y}\right]_k + z_k \cdot [K] - \left[\alpha_{x-y}\right]_k \cdot \Delta T\right) \quad (3\text{-}14)$$

Where $\left[\sigma_{x-y}\right]_k$ are the thermal expansion coefficients of the *kth* layer and ΔT is the change in temperature.

Rather than dealing with each layer in the laminate individually, we can use a plate force and plate moment that applies to the entire laminate. This method requires finding a laminate stiffness matrix. The plate forces can be found by integrating the stress of each lamina over the lamina thickness $t_k = (h_k - h_{k-1})$ and summing the results. Plate moments can be found in a similar way by including the distance from the mid-plane as a lever arm.

$$\begin{Bmatrix} N_x \\ N_y \\ N_{xy} \end{Bmatrix} = \sum_{k=1}^{n} \int_{h_{k-1}}^{h_k} \begin{Bmatrix} \sigma_x \\ \sigma_y \\ \tau_{xy} \end{Bmatrix}_k \cdot dz \quad (3\text{-}15)$$

$$\begin{Bmatrix} M_x \\ M_y \\ M_{xy} \end{Bmatrix} = \sum_{k=1}^{n} \int_{h_{k-1}}^{h_k} \begin{Bmatrix} \sigma_x \\ \sigma_y \\ \tau_{xy} \end{Bmatrix}_k \cdot z dz \quad (3\text{-}16)$$

Equation (3-14) can be substituted into Equations (3-15) and (3-16) to form:

$$[N] = [A][\varepsilon^0] + [B][K] - [N]^T \quad (3\text{-}17)$$
$$[M] = [B][\varepsilon^0] + [D][K] - [M]^T \quad (3\text{-}18)$$

These two relationships can be written as one matrix equation with a 6x6 laminate stiffness matrix.

$$\begin{bmatrix}\bar{N}\\ \bar{M}\end{bmatrix} = \begin{bmatrix}A & B\\ B & D\end{bmatrix} \cdot \begin{bmatrix}\varepsilon^0\\ K\end{bmatrix} \tag{3-19}$$

$$[A] = \sum_{k=1}^{n} \left[\bar{Q}_{x-y}\right]_k \cdot t_k \tag{3-20}$$

$$[B] = \sum_{k=1}^{n} \left[\bar{Q}_{x-y}\right]_k \cdot t_k \cdot \bar{h}_k \tag{3-21}$$

$$[D] = \sum_{k=1}^{n} \left[\bar{Q}_{x-y}\right]_k \cdot \left(t_k \cdot \bar{h}_k^2 + \frac{1}{2} \cdot t_k^3\right) \tag{3-22}$$

Where $\bar{h}_k = \frac{h_k + h_{k-1}}{2}$.

$$[N]^T = \Delta T \cdot \sum_{k=1}^{n} \left[\bar{Q}_{x-y}\right]_k \cdot \left[\alpha_{x-y}\right]_k \cdot (h_k - h_{k-1}) \tag{3-23}$$

$$[M]^T = \frac{\Delta T}{2} \cdot \sum_{k=1}^{n} \left[\bar{Q}_{x-y}\right]_k \cdot \left[\alpha_{x-y}\right]_k \cdot (h_k^2 - h_{k-1}^2) \tag{3-24}$$

$$[\bar{N}] = [N] + [N]^T \tag{3-25}$$

$$[\bar{M}] = [M] + [M]^T \tag{3-26}$$

Each matrix within $\begin{bmatrix}A & B\\ B & D\end{bmatrix}$ represents a grouping of stiffness relationships. The $[A]$ matrix corresponds to the extensional stiffness, the $[B]$ matrix corresponds to the extensional-bending coupling stiffness, and the $[D]$ matrix corresponds to the bending stiffness. In particular, the D_{22} value corresponds to the bending stiffness in the y-direction.

Chapter 4

Results of Spring-in FE Analysis

The finite element model developed and validated in Chapter 2 was used to analyze the effect of selected structural parameters on the spring-in of the composite sandwich panel described in Chapter 2. The method for measuring spring-in gap distance used here is the same as that used by Mahadik and Potter [3] and explained in Section 2.7. The temperature delta is -50°F as described in Section 2.6. The spring-in gap measurements of each case are presented in this chapter along with a short discussion.

4.1 Effect of Core Thickness on Spring-in

Several different core thicknesses were analyzed using a common symmetric face sheet lay-up of $[0°/90°/0°/90°/Core/90°/0°/90°/0°]_T$ with the core thickness ranging from 0.005 inches (the thickness of one ply of graphite fiber) to 0.5 inches. The resulting spring-in gap is then presented in Figure 4-1. Plotted on the right axis is the bending stiffness (D_{22}) calculated using classical lamination theory for the total material stack up.

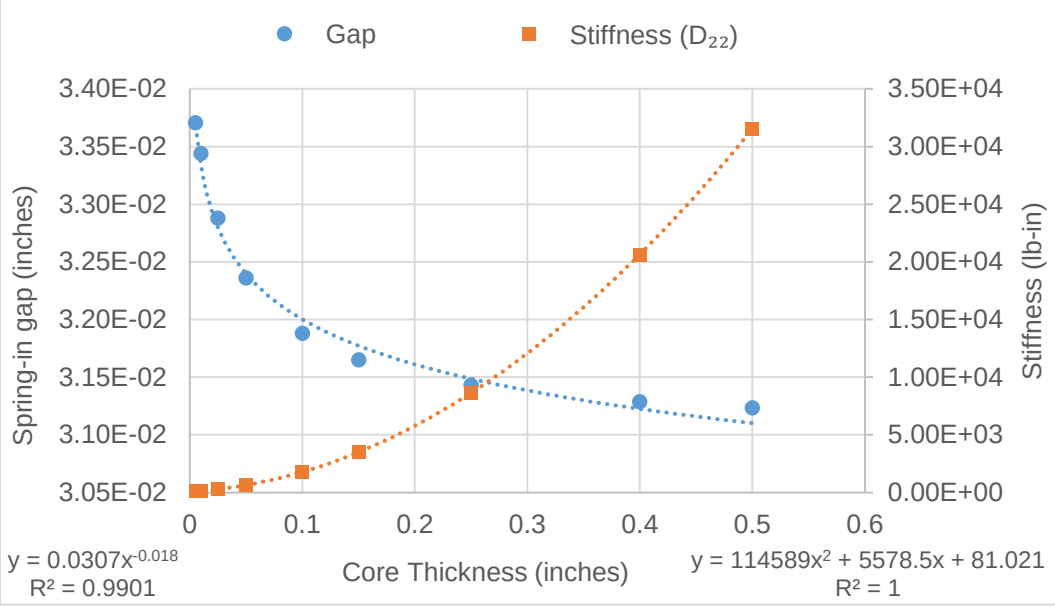

Figure 4-1 Spring-in of sandwich panel with varying core thickness

It was found that the spring-in gap decreases as the core increases in thickness for this specific face sheet layup. This result is expected since a thicker core results in a greater bending stiffness.

4.2 Effect of Face Sheet Thickness on Spring-in

A second case was investigated using a constant core thickness of 0.5 inches with variable, but symmetric, face sheet thickness. A layup pattern of $[(0°/90°)_x/0.5\text{Core}/(90°/0°)_x]_T$ is used for this analysis with the variable "x" ranging from 2 to 18 for a total of 4 to 36 plies per face sheet. The plot in Figure 4-2 shows the number of plies in one face sheet on the horizontal axis and the spring-in gap measurement on the vertical axis. For example: 4 plies = $[(0°/90°)_2/0.5\text{Core}/(90°/0°)_2]_T$, where 4 plies corresponds to the number of plies in one face sheet's $[0°/90°/0°/90°]_T$ layup.

Increased face sheet thickness results in increased spring-in gap distance for this specific face sheet layup and core thickness. Figure 4-2 shows that spring-in increases as the ply thickness increases and the thermal induced load N^T_y becomes a larger negative value.

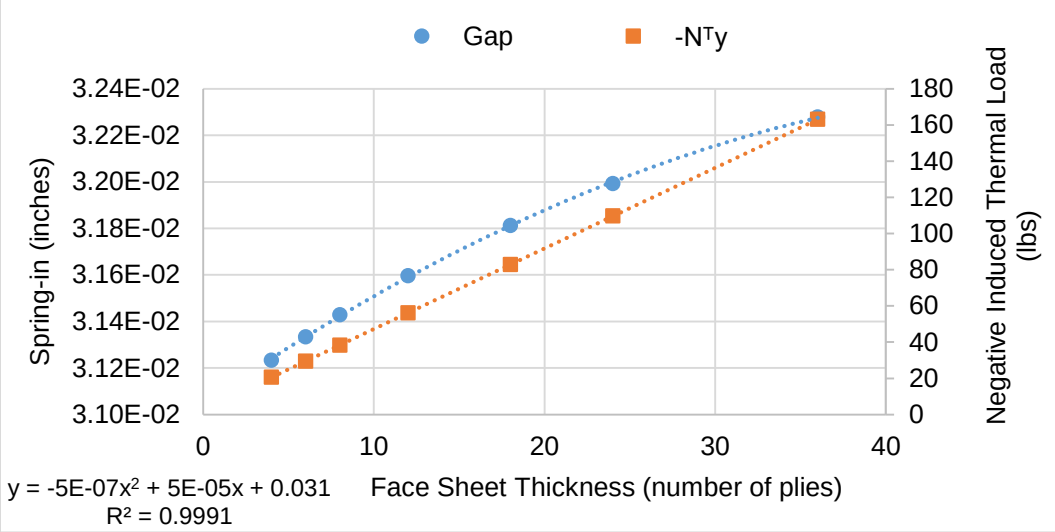

Figure 4-2 Spring-in of sandwich panel with varying face sheet thickness

4.3 Effect of Quasi-Isotropic Layups on Spring-in

Other quasi-isotropic layups besides the cross-ply [0°/90°] layup were investigated including $[0°/\pm60°/0.5\text{Core}/\mp60°/0°]_T$, $[0°/\pm45°/90°/0.5\text{Core}/90°/\mp45°/0°]_T$, and $[0°/\pm30°/\pm60°/90°/0.5\text{Core}/90°/\mp60°/\mp30°/0°]_T$. Equation (4-1) shows the formula for calculating quasi-isotropic layups where "*S*" is the total number of different fiber orientations and "*k*" is the ply number from 1 to *S*.

$$\theta_k = \frac{(k-1)\pi}{S} \tag{4-1}$$

Table 4-1 lists the three previously mentioned quasi-isotropic layups plus a few additional layups and their corresponding spring-in gap measurements. The table subsequently lists the spring-in gap measurement of the same thickness but with a $[0°/90°]_x$ face sheet layup which was presented in Section 4.2.

The results of the analysis are within 0.1% between the quasi-isotropic layup and the $[0°/90°]_x$ layup. These results show that the spring-in gap distance is only dependent on the number of plies in the face sheet for quasi-isotropic layups. The spring-in gap measurements of the quasi-isotropic face sheet layups are nearly equivalent to the $[0°/90°]_x$ face sheet layups of the same number of plies per face sheet.

Table 4-1 Quasi-isotropic face sheet ply layup compared to $[0/90]_x$ layup of same thickness

# Plies	Layup	Spring-in Gap (inches)
3	$[0°/\pm60°/0.5\text{Core}/\mp60°/0°]_T$	3.1174E-02
	-	
4	$[0°/\pm45°/90°/0.5\text{Core}/90°/\mp45°/0°]_T$	3.1226E-02
6	$[0°/\pm30°/\pm60°/90°/0.5\text{Core}/90°/\mp60°/\mp30°/0°]_T$	3.1322E-02
8	$[((k\text{-}1)\pi/8)_{k=1\text{-}8}/0.5\text{Core}/-((k\text{-}1)\pi/8)_{k=1\text{-}8}]_T$	3.1416E-02
12	$[((k\text{-}1)\pi/12)_{k=1\text{-}12}/0.5\text{Core}/-((k\text{-}1)\pi/12)_{k=1\text{-}12}]_T$	3.1579E-02
	-	-
4	$[(0°/90°)_2/0.5\text{Core}/(90°/0°)_2]_T$	3.1228E-02
6	$[(0°/90°)_3/0.5\text{Core}/(90°/0°)_3]_T$	3.1322E-02
8	$[(0°/90°)_4/0.5\text{Core}/(90°/0°)_4]_T$	3.1428E-02
12	$[(0°/90°)_6/0.5\text{Core}/(90°/0°)_6]_T$	3.1596E-02

4.4 Effect of Angled Ply Layups on Spring-in

In this analysis, angled ply layups in increments of 15° orientations are investigated. Each layup used in this analysis consists of 4-ply face sheets of balanced angled plies and a 0.5-inch core: $[(\pm X°)_2/0.5\text{Core}/(\mp X°)_2]_T$ with the orientation "$X°$" being one of the 15° increments. This layup pattern results in a symmetric and balanced structure.

Figure 4-3 shows that the greatest spring-in occurs when the angled plies near 45°. It should be noted that N_x^T and N_y^T are equal for this face sheet laminate. The lowest spring-in occurs when the angled plies approach 0° and 90°, with 90° resulting in a slightly lower spring-in gap distance than 0°. The effect may be due to an interaction between bending stiffness and the thermal induced load. Further investigation is required.

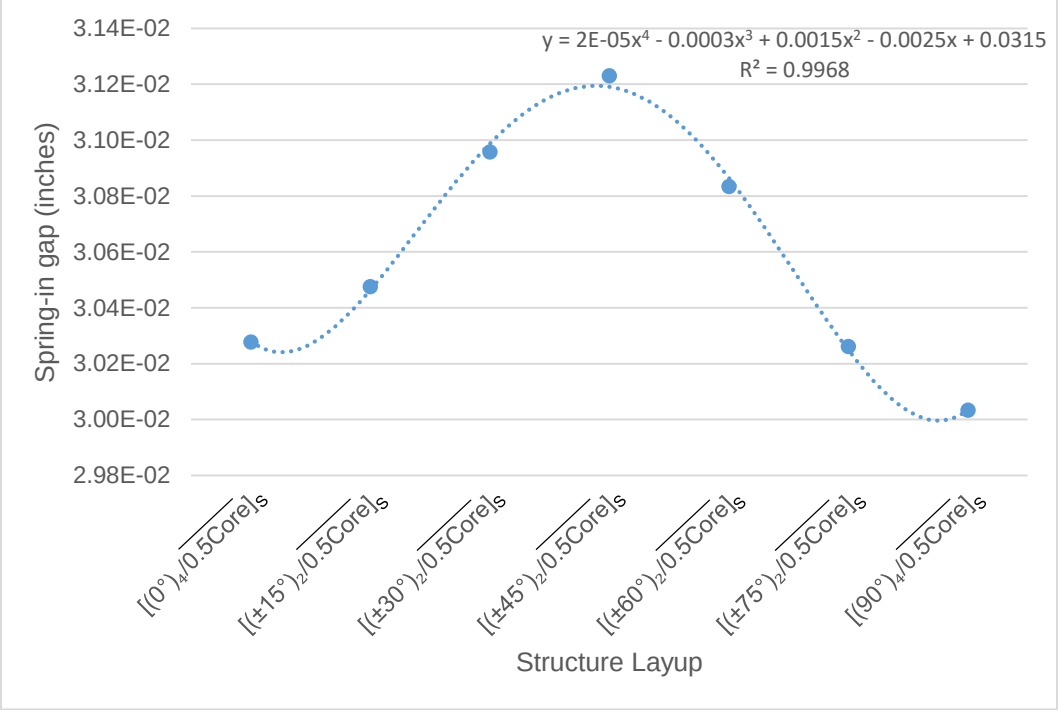

Figure 4-3 Spring-in of sandwich panel with various balanced and symmetric angled ply layups

4.5 Effect of Asymmetric Face Sheets on Spring-in

This case focuses on analyzing the effect of using two face sheets that are not symmetric about the centerline of the structure. The basic layup of the structure for this case will be $[\pm45°/0°/90°/0.5Core/90°/0°/\mp45°]_T$, a symmetric face sheet structure. This basic face sheet layup will be doubled and tripled for one face sheet only to see its effect on the spring-in of the structure relative to the basic layup. Now that symmetric layups are not being used, the order of the ply orientations relative to the global laminate coordinate system become important. The laminate orientation code reads from left to right as inner-side of the curved shape to outer-side (tool-side). The results, as seen in Figure 4-4, show that spring-in decreases when the tool-side face sheet thickness is

thicker than the inner-side face sheet. This effect is due to the increased thermal induced load due to the -ΔT on the tool-side face sheet counteracting the spring-in force.

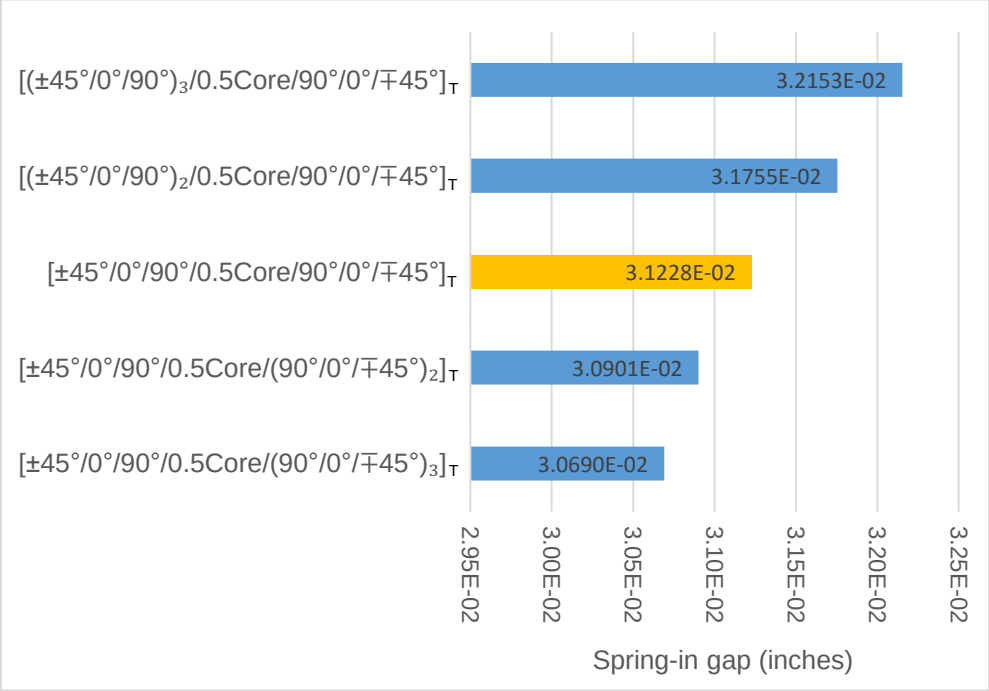

Figure 4-4 Effect of asymmetric face sheet thickness on spring-in

Next, the basic structure spring-in is compared to the spring-in of two asymmetric face sheets with an equal number of plies. Figure 4-5 shows that spring-in decreases when the ±45° plies are biased toward the tool side. The asymmetric stacking sequence results in a thermal induced moment that increases or decreases the spring-in depending on the direction.

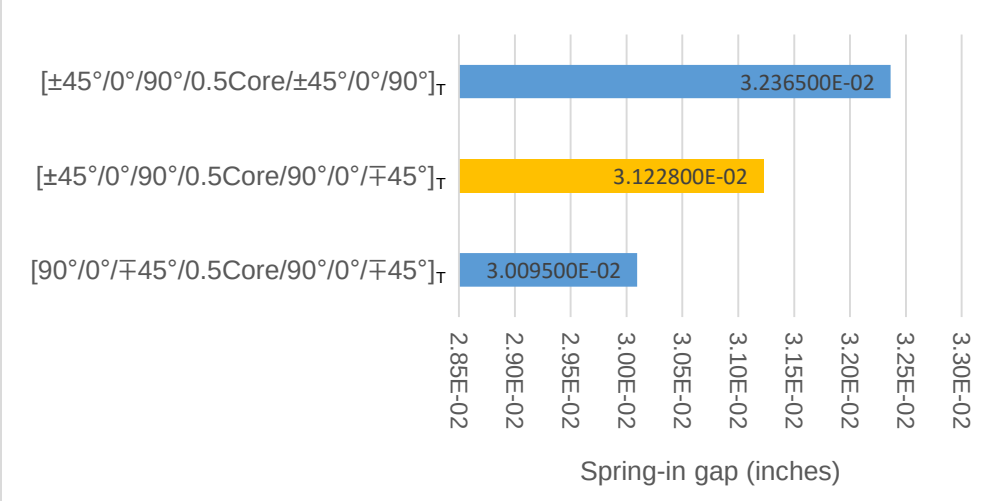

Figure 4-5 Effect of opposite/asymmetric face sheets with equal thickness on spring-in

4.6 Effect of Structure Radius on Spring-in

Three different radii were investigated to determine their effect on spring-in for a $[(0°/90°)_2/0.5\text{Core}/(90°/0°)_2]_T$ laminate. Radii of 16, 8, and 4 inches are used, keeping the mesh element size the same as the mesh described in Section 2.3, resulting in a 12xN mesh where N varies depending on the length around the structure's curved length. It was found that spring-in increases linearly as the structure radius increases for a constant ΔT. All radii use the same layup and therefore have equivalent thermal induced loads. This thermal induced load acted on the longer curved lever arm of the larger radius shapes result in greater spring-in.

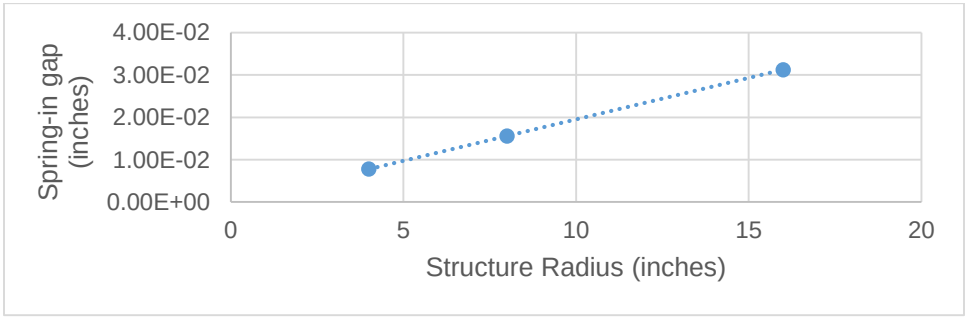

Figure 4-6 Effect of structure radius on spring-in

4.7 Effect of Temperature Change on Spring-in

Three different temperatures were investigated using a $[(0°/90°)_2/0.5Core/(90°/0°)_2]_T$ laminate to determine their effect on spring-in. Temperatures of -50°F, -100°F, and 150°F were chosen. The results appear as expected since spring-in normally occurs when cooling a curved composite structure after curing; therefore, a greater negative temperature change should result in a greater spring-in gap distance. The temperature change appears to have a linear effect on the spring-in gap distance. Doubling the temperature delta from -50°F to -100°F results in a doubling of the spring-in gap distance. Tripling the temperature delta from -50°F to -150°F results in a tripling of the spring-in gap distance.

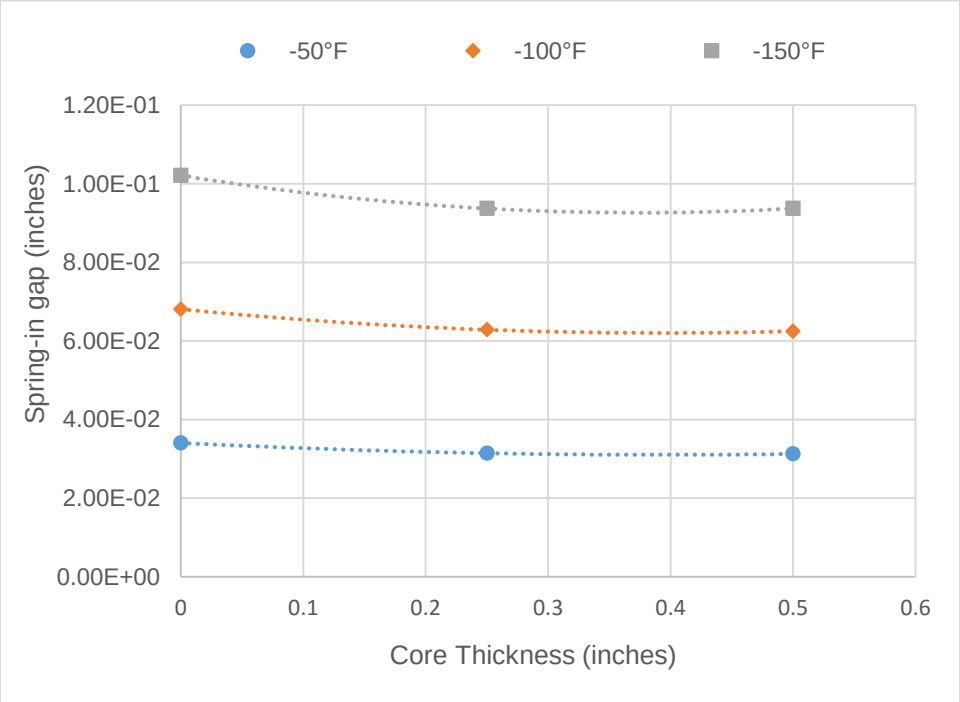

Figure 4-7 Effect of temperature on spring-in

Chapter 5

Conclusions

A finite element model of a curved composite sandwich panel was developed in ANSYS and validated by comparison to published experimental results. This model was then used to find the total spring-in gap distance of the structure caused by thermal deformation when subjected to a $-\Delta T$. Model cases were run for several different varying structural parameters and the following general conclusions were made:

When varying core thickness, it was found that spring-in decreases as core thickness and bending stiffness increase for a $[(0°/90°)_2/\text{Core}/(90°/0°)_2]_T$ laminate.

When varying face sheet thickness for a $[(0°/90°)_x/0.5\text{Core}/(90°/0°)_x]_T$ laminate, spring-in increases as face sheet thickness increases.

Quasi-isotropic layups result in spring-in that increases as the face sheet thickness increases. The quasi-isotropic spring-in gap distances are nearly identical to the corresponding $[(0°/90°)_x/0.5\text{Core}/(90°/0°)_x]_T$ layup spring-in gap distances previously measured.

Looking at angled ply laminates of the formula $[(\pm X°)_2/0.5\text{Core}/(\mp X°)_2]_T$, spring-in was found to increase when "X°" neared 45° and decrease as "X°" neared 0° and 90°.

Asymmetric face sheet thicknesses were found to cause greater spring-in with the thicker face sheet on the inner-side of the structure and less spring-in with a thicker face sheet on the tool-side for a $[(\pm45°/0°/90°)_x/0.5\text{Core}/(90°/0°/\mp45°)_x]_T$ laminate.

Running two opposite asymmetric laminates, $[\pm45°/0°/90°/0.5\text{Core}/\pm45°/0°/90°]_T$ and $[90°/0°/\mp45°/0.5\text{Core}/90°/0°/\mp45°]_T$, with equal face sheet thickness resulted in less spring-in when the ±45° plies were biased toward the tool-side.

Varying the structure radius has an approximately linear effect on the spring-in gap distance. Spring-in increases as structure radius increases.

The temperature delta has an approximately linear effect on the spring-in gap distance for a $[(0°/90°)_2/0.5Core/(90°/0°)_2]_T$ laminate. When doubling and tripling the temperature delta, the spring-in gap distance doubles and triples as well.

Appendix A

General ANSYS Curved Composite Sandwich Panel Model

```
!ANSYS_CODE.TXT
! /COM,ANSYS RELEASE Release 16.2 BUILD 16.2 UP20150629
/PREP7
/RGB,INDEX,100,100,100, 0
/RGB,INDEX, 80, 80, 80,13
/RGB,INDEX, 60, 60, 60,14
/RGB,INDEX, 0, 0, 0,15

!Create keypoints to make arcs
K,1,-16,-16,0,
K,2,0,0,0,
K,3,16,-16,0,
K,4,-16,-16,24,
K,5,0,-16,0,

!Make arcs with 16" radius
LARC,1,2,5,16,
LARC,2,3,5,16,

!Make straight line extrusion axis
LSTR,       1,       4

!Extrude curves
FLST,2,2,4,ORDE,2
FITEM,2,1
FITEM,2,-2
ADRAG,P51X, , , , , ,       3

!Create element type
ET,1,SHELL281

!Mesh areas
FLST,5,2,5,ORDE,2
FITEM,5,1
FITEM,5,-2
CM,_Y,AREA
ASEL, , , ,P51X
CM,_Y1,AREA
CHKMSH,'AREA'
CMSEL,S,_Y
CMDELE,_Y
AMESH,_Y1
CMDELE,_Y1

!Refine mesh to level 3
FLST,5,72,2,ORDE,2
FITEM,5,1
FITEM,5,-72
CM,_Y,ELEM
ESEL, , , ,P51X
```

```
CM,_Y1,ELEM
CMSEL,S,_Y
CMDELE,_Y
EREF,_Y1, , ,3,0,1,1
CMDELE,_Y1

!Refine mesh level 1
FLST,5,288,2,ORDE,2
FITEM,5,1
FITEM,5,-288
CM,_Y,ELEM
ESEL, , , ,P51X
CM,_Y1,ELEM
CMSEL,S,_Y
CMDELE,_Y
EREF,_Y1, , ,1,0,1,1
CMDELE,_Y1

!Corner nodes 1,14,56,50
!Corner nodes 1,14,47,41 for shell281

!Set material properties for lamina
MPTEMP,,,,,,,,
MPTEMP,1,0
MPDATA,EX,1,,2.13E+07
MPDATA,EY,1,,1.50E+06
MPDATA,EZ,1,,1.50E+06
MPDATA,PRXY,1,,0.27
MPDATA,PRYZ,1,,0.54
MPDATA,PRXZ,1,,0.27
MPDATA,GXY,1,,1.00E+06
MPDATA,GYZ,1,,5.40E+05
MPDATA,GXZ,1,,1.00E+06
MPTEMP,,,,,,,,
MPTEMP,1,0
UIMP,1,REFT,,,
MPDATA,CTEX,1,,-5.00E-07
MPDATA,CTEY,1,,1.50E-05
MPDATA,CTEZ,1,,1.50E-05

!Set material properties for core
MPTEMP,,,,,,,,
MPTEMP,1,0
MPDATA,EX,2,,10
MPDATA,EY,2,,10
MPDATA,EZ,2,,1.70E+04
MPDATA,PRXY,2,,0.1
MPDATA,PRYZ,2,,0.01
MPDATA,PRXZ,2,,0.01
MPDATA,GXY,2,,10
```

```
MPDATA,GYZ,2,,3.50E+03
MPDATA,GXZ,2,,5.60E+03
MPTEMP,,,,,,,,
MPTEMP,1,0
UIMP,2,REFT,,,
MPDATA,CTEX,2,,1.00E-08
MPDATA,CTEY,2,,1.00E-08
MPDATA,CTEZ,2,,1.94E-05

!Set section data, tool-side first
sect,1,shell,,
secdata, .005,1,0,3
secdata, .005,1,90,3
secdata, .005,1,0,3
secdata, .005,1,90,3
secdata, .5,2,0,3
secdata, .005,1,90,3
secdata, .005,1,0,3
secdata, .005,1,90,3
secdata, .005,1,0,3
secoffset,MID
seccontrol,,,, , , ,

!Set allDOF constraint at 0,0,0
FLST,2,1,3,ORDE,1
FITEM,2,2
/GO
DK,P51X, , , ,0,ALL, , , , , ,

!Set temperature delta -50
FLST,2,2,5,ORDE,2
FITEM,2,1
FITEM,2,-2
BFA,P51X,TEMP,-50

!Solve
FINISH
/SOL
SOLVE
FINISH
/POST1

!Output data to file
/output,PRNSOL,lis
PRNSOL,U,COMP
/out
```

Appendix B

MATLAB Code for Calculating [A], [B], [D] Matrix

```
function [A,B,D] = calculateABD(lam)
%calculateABD: Assembles A B D matrices for laminate given lamina
% properties

%{
Example Laminate [0_2/45_2]T
lam=[E1,E2,v12,G12,tply,0;          %k1
     E1,E2,v12,G12,tply,0;          %k2
     E1,E2,v12,G12,tply,45*pi/180;  %k3
     E1,E2,v12,G12,tply,45*pi/180]  %k4
%}

%Create output matrices with zeros
lamSize=size(lam);
A=zeros(3,3);
B=zeros(3,3);
D=zeros(3,3);
h_bar=zeros(lamSize(1,1),1);

%Create a [k x 1] matrix of h_bar values with origin at bottom of
% laminate
%k=kth lamina
for k=1:1:lamSize(1,1)
    %Add current lamina thickness and all previous lamina
    %j=first lamina through kth lamina
    for j=1:1:k
        h_bar(k,1)=h_bar(k,1)+lam(j,5);
    end
    %Subtract half of kth lamina thickness to get midplane of
      % lamina
    t=lam(k,5);
    h_bar(k,1)=h_bar(k,1)-t/2;
end
%Subtract laminate thickness divided by 2 to get h from laminate
%mid-plane
h_bar=h_bar-((h_bar(end,1)+lam(end,5)/2)/2);

%Cycle through each lamina and calculate Q and add to A, B, D
% matrices
%k=kth lamina
for k=1:1:lamSize(1,1)
    E1=lam(k,1);
    E2=lam(k,2);
    v12=lam(k,3);
    G12=lam(k,4);
    t=lam(k,5);
    theta=lam(k,6);

    Q=Qbar(E1,E2,v12,G12,theta);
```

```
50
51          A=A+(Q.*t);
52          B=B+(Q.*t.*h_bar(k,1));
53          D=D+(Q.*(t*h_bar(k,1)*h_bar(k,1)+1/12*t^3));
54      end
55
56      %Set very small values to zero
57      if abs(A(1,3)/A(1,1))<1E-6
58          A(1,3)=0;
59          A(3,1)=0;
60      end
61
62      if abs(A(2,3)/A(1,1))<1E-6
63          A(2,3)=0;
64          A(3,2)=0;
65      end
66
67      for i=1:1:3
68          for j=1:1:3
69              if abs(B(i,j)/A(1,1))<1E-6
70                  B(i,j)=0;
71              end
72          end
73      end
74
75      if abs(D(1,3)/D(1,1))<1E-6
76          D(1,3)=0;
77          D(3,1)=0;
78      end
79
80      if abs(D(2,3)/D(1,1))<1E-6
81          D(2,3)=0;
82          D(3,2)=0;
83      End
84
85
86      function [Qbar] = Qbar(E1,E2,v12,G12,theta)
87      %Qbar assembles reduced stiffness matrix for theta (rad) ply
88
89      v21=E2*v12/E1; %Poisson's ratio, loaded in 2-direction, deformed
90                        % in 1-direction
91
92      Q11=E1/(1-v12*v21);
93      Q22=E2/(1-v12*v21);
94      Q12=v12*E2/(1-v12*v21);
95      Q66=G12;
96
97      m=cos(theta);
98      n=sin(theta);
```

```
 99
100   Qxx=m^4*Q11+n^4*Q22+2*(Q12+2*Q66)*m*m*n*n;
101   Qyy=n^4*Q11+m^4*Q22+2*(Q12+2*Q66)*m*m*n*n;
102   Qxy=m*m*n*n*(Q11+Q22-4*Q66)+(m^4+n^4)*Q12;
103   Qxs=m^3*n*(Q11-Q12-2*Q66)-m*n^3*(Q22-Q12-2*Q66);
104   Qys=m*n^3*(Q11-Q12-2*Q66)-m^3*n*(Q22-Q12-2*Q66);
105   Qss=m*m*n*n*(Q11+Q22-2*Q12-2*Q66)+(m^4+n^4)*Q66;
106
107   Qbar=[Qxx Qxy Qxs;
108      Qxy Qyy Qys;
109      Qxs Qys Qss];
110
111   %Set very small values to zero
112   if abs(Qbar(1,3)/Qbar(1,1))<1E-6
113       Qbar(1,3)=0;
114       Qbar(3,1)=0;
115   end
116
117   if abs(Qbar(2,3)/Qbar(1,1))<1E-6
118       Qbar(2,3)=0;
119       Qbar(3,2)=0;
120   end
```

Appendix C

MATLAB Code for Calculating [N^T] Matrix

```
function [NT] = calculateNT(lam)
%calculateNT: Assembles NT matrices for laminate given lamina
properties

%{
Example Laminate [0_2/45_2]T
lam=[E1,E2,v12,G12,tply,0;          %k1
     E1,E2,v12,G12,tply,0;          %k2
     E1,E2,v12,G12,tply,45*pi/180;  %k3
     E1,E2,v12,G12,tply,45*pi/180]  %k4
%}

%Create output matrices with zeros
lamSize=size(lam);
NT=zeros(3,1);

%Cycle through each lamina and calculate Q and add to NT matrices
%k=kth lamina
for k=1:1:lamSize(1,1)
    E1=lam(k,1);
    E2=lam(k,2);
    v12=lam(k,3);
    G12=lam(k,4);
    t=lam(k,5);
    theta=lam(k,6);
    deltaT=lam(k,7);
    alpha1=lam(k,8);
    alpha2=lam(k,9);

    m=cos(-theta);
    n=sin(-theta);
    T=[m*m n*n m*n; n*n m*m -m*n;-2*m*n 2*m*n m*m-n*n];

    Q=Qbar(E1,E2,v12,G12,theta);
    alpha=T*[alpha1;alpha2;0];

    NT=NT+(Q*alpha*t*deltaT);
end
```

References

[1] Albert, C. and Fernlund, G., “Spring-in and warpage of angled composite laminates”, Composites Science and Technology, Vol. 62, 2002, pp.1895-1912.

[2] Fernlund, G., "Spring-in of angled sandwich panels", Composites Science and Technology, Vol. 65.2, 2005, pp.317-323.

[3] Mahadik, Y. and Potter, K., "Experimental investigation into the thermoelastic spring-in of curved sandwich panels", Composites Part A: Applied Science and Manufacturing, Vol. 49, 2013, pp.68-80.

[4] Black, J. et al., “Experimental Investigation of Spring-in Behavior of Composite Laminates for Proceedings of the American Society for Composites 27th Annual Technical Conference/15th US-Japan Conference on Composites”, 2012.

[5] Kappel, E., “Spring-in of curved CFRP/foam-core sandwich structures”, Composite Structures, Vol. 128, 2015, pp.155-164.

[6] “ANSYS Mechanical APDL Element Reference”, Release 15.0, 2013.

[7] Daniel, I.M. and Ishai, O., *Engineering Mechanicas of Composite Materials*, 2nd Ed., Oxford University Press, New York, 2006, p.380.

[8] Hexcel, 6 April 2016, “HRH-10 Product Data”, <http://www.hexcel.com/Resources/DataSheets/Honeycomb-Data-Sheets/HRH_10_us.pdf>.

[9] Hexcel, 6 April 2016, “Honeycomb Attributes and Properties”, <http://www.hexcel.com/Resources/DataSheets/Brochure-Data-Sheets/Honeycomb_Attributes_and_Properties.pdf>.

[10] Hexcel, 6 April 2016, “Honeycomb Sandwich Design Technology”, <http://www.hexcel.com/Resources/DataSheets/Brochure-Data-Sheets/Honeycomb_Sandwich_Design_Technology.pdf>.

[11] Chan, W. S., ME5315 Class Notes, 2014.

Biographical Information

Brady C. Lotz received his Bachelor of Science degree in Aerospace Engineering at the University of Texas at Austin in December 2008. He then entered the workforce at L-3 Communications in Greenville, TX as a structural design engineer. After five years at L-3, Brady began studies at the University of Texas at Arlington, where he received his Master of Science degree in Mechanical Engineering in May 2016. His academic interests include composites and structural design. Brady remains employed at L-3 Communications as a structural design engineer.